Journal of Solid State Chemistry 184 (2011) 852–858

Contents lists available at ScienceDirect

Journal of Solid State Chemistry

journal homepage: www.elsevier.com/locate/jssc

$K_2Mg_{5-x}Sn_3$ and $K_3Mg_{18}Tt_{11}$ (Tt=Sn, pb) with two types of Mg–Sn/Pb frameworks

Xiao-Wu Lei

Department of Chemistry and Chemical Engineering, Jining University, Qufu, Shandong 273155, China

ARTICLE INFO

Article history:
Received 24 August 2010
Received in revised form
19 January 2011
Accepted 6 February 2011
Available online 12 February 2011

Keywords:
Intermetallics
Crystal structures
Stannides
Electronic structure calculations

ABSTRACT

$K_2Mg_{5-x}Sn_3$ (x=0.28) and $K_3Mg_{18}Tt_{11}$ (Tt=Sn, Pb) have been synthesized by reacting the mixture of the corresponding pure elements at high temperature, and structurally characterized by single-crystal X-ray diffraction studies. $K_2Mg_{5-x}Sn_3$ (x=0.28) is isostructural with $Ni_{7-x}SbQ_2$ (Q=Se, Te) series and features 2D corrugated $[Mg_{5-x}Sn_3]$ layers that are separated by K^+ cations. The structure of $K_3Mg_{18}Tt_{11}$ (Tt=Sn, Pb) is closely related to the $Ho_2Rh_{12}As_7$ structural type and features 3D $[Mg_{18}Tt_{11}]$ framework composed of 1D $[Mg_{18}Tt_{11}]$ columns that are interconnected via Mg–Tt bonds, forming 1D hexagonal tunnels occupied by the K+ cations. Electronic structure calculations indicate that Mg atoms can function as either electron donor or as a participator in the network along with Tt atoms. Magnetic property measurements and band structure calculations indicate that these compounds are metallic.

1. Introduction

Intermetallics formed by alkali metal (alkaline earth or rare earth metal) and group 14 elements (tetrels, Tt=Si, Ge, Sn, Pb) have been extensively investigated because of their rich structural diversities and novel chemical bonding [1–7]. Many types of anionic Tt oligomers, chains, clusters and nets have been found in these binary phases [8–28]. In addition, the strategy of using mixed cations that differ in size and/or charge has been proven to be an effective route to novel clusters or extended structures that cannot be isolated by using only one type of cation [29–32]. For example, $A_4Li_2Sn_8$ (A=K, Rb) feature isolated arachno-cluster of $[Sn_8]^{6-}$ with shape of square antiprism, and $RbLi_7Ge_8$ contains an isolated giant cluster of $[Ge_{12}]^{12-}$ with shape of truncated tetrahedron [29–30]. It should be noted that the lithium cation in these compounds not only reduces the p-elements, but also participates in the formation of anionic frameworks. They cap the square faces of $[Sn_8]^{6-}$ and hexagonal faces of $[Ge_{12}]^{12-}$ into "closed" $[Li_2Sn_8]^{4-}$ and $[Li_4Ge_{12}]^{8-}$ clusters.

In recent years, the systematic research in alkaline earth (or rare earth)–Mg–Tt systems has shown that the magnesium atom is also capable of participating in the formation of anionic skeletons as lithium. Several such examples include AeMgTt (Ae=Ca, Sr; Tt=Si, Ge, Sn) featuring a 3D network based on 1D [MgTt] ladders [33]; $BaMg_2Tt_2$ (Tt=Si, Ge, Sn, Pb) series feature three types of 3D framework composed of 2D corrugated $[Mg_2Tt_2]$ layers interconnected via Mg–Tt and/or Tt–Tt bonds/bond [34]; $BaMg_4Tt_3$ (Tt=Si, Ge) feature a novel structure type different from the isoelectronic Zintl phases of Ba_5Tt_3 (Ba_5Si_3 type) [35–37]; and RE_2MgGe_2 (RE=Y, La–Nd, Sm, Gd, Tb) and Yb_4MgGe_4 both containing flat $[MgGe_2]$ layers, which can be considered as $[Ge_2]^{6-}$ dimers interconnected by Mg atoms via Mg–Ge bonds [38,39]. Many other such phases have also been isolated, such as $Ae_5Mg_{18}Tt_{13}$ (Ae=Sr, Ba; Tt=Si, Ge) [40], $Sr_{13}Mg_2Si_{20}$ [41], $Ba_2Mg_3Si_4$ [42], $Ca_7Mg_{7.5+\delta}Si_{14}$ [43], $Ca_{6.2}Mg_{3.8}Sn_7$ [44], $Ba_2Mg_{12}Ge_{7.33}$ [45] and so on [46–48]. A few ternary phases in the A–Mg–Tt (A represents an alkali metal) system have been prepared and their structures elucidated, including Li_2MgTt (Tt=Si, Ge, Sn, Pb) [49], $Li_2Mg_3Si_4$ [50] and Li_8MgSi_6 [51].

So far, no compound in the K–Mg–Tt system has been reported. Our explorations in this system led to three new phases, namely $K_2Mg_{5-x}Sn_3$ (x=0.28) and $K_3Mg_{18}Tt_{11}$ (Tt=Sn, Pb), and their structures feature 2D $[Mg_5Sn_3]$ layers and 3D $[Mg_{18}Tt_{11}]$ network, respectively. Herein, we report their crystal structures, chemical bonding and physical properties.

2. Experimental section

2.1. Materials and instrumentation

All manipulations were performed within an argon-filled glove-box with a moisture level below 1 ppm. All chemicals were used as received: potassium blocks (Shanghai fourth chemical reagent company, 99.99%), magnesium pieces (Acros, 99.99%), Sn granules (Acros, 99.99%) and Pb powder (Acros, 99.99%). Semi-quantitative microprobe elemental analyses for K, Mg, Sn

E-mail address: xwlei10@163.com

0022-4596/$ - see front matter Crown Copyright © 2011 Published by Elsevier Inc. All rights reserved.
doi:10.1016/j.jssc.2011.02.003

and Pb atoms were performed on a JSM-6700F scanning electron microscope (SEM) equipped with an energy dispersive spectroscope (EDS) detector. The X-ray diffraction (XRD) powder patterns were collected at room temperature on an X'Pert-Pro diffractometer using Cu $K\alpha$ radiation ($\lambda=1.5406$ Å) in the 2θ range 5–70° with a step size of 0.04° and 10 s/step counting time. Magnetic susceptibility measurements of the powder samples were performed on a Quantum Design PPMS-9T magnetometer at a field of 5000 Oe in the temperature range 5–310 K.

2.2. Preparation of $K_2Mg_{5-x}Sn_3$ ($x=0.28$)

Single crystals of $K_2Mg_{5-x}Sn_3$ ($x=0.28$) were initially obtained by reacting the mixture of K, Mg and Sn metals in molar ratio of 1:2:2. The samples were loaded into a tantalum tube, which was subsequently arc-welded under an argon atmosphere and sealed in a quartz tube under vacuum ($\sim10^{-4}$ Torr). The reaction was performed at 800 °C for 7 days with prior heating at 300 °C for 1 day. After the heat treatment, the tube was allowed to cool slowly, at a controlled rate of 0.1 °C/min, to room temperature. Plate-shaped single crystals of $K_2Mg_{5-x}Sn_3$ ($x=0.28$) were selected and used for the structural analyses. The compound is air and moisture-sensitive. Microprobe elemental analyses on clean surfaces of several single crystals of $K_2Mg_{5-x}Sn_3$ indicated the presence of K, Mg and Sn elements in an average molar ratio of 2.0(8):5.0(5):3.3(6), which were in good agreement with results derived from single-crystal X-ray diffraction refinement. After proper structural analyses, the compound was prepared in a high yield and high purity by reacting a mixture of the pure metals in tantalum tubes according to the loading composition of "$K_2Mg_5Sn_3$". The sample was reacted at 800 °C for 2 days and then annealed at 500 °C for 7 days. The measured X-ray diffraction powder pattern matches well with the one simulated from the single-crystal X-ray structural analysis (see Appendix A).

2.3. Preparation of $K_3Mg_{18}Tt_{11}$ (Tt=Sn, Pb)

Single crystals of $K_3Mg_{18}Sn_{11}$ and $K_3Mg_{18}Pb_{11}$were initially obtained by reacting the mixture of K, Mg and Sn (or Pb) metals in the molar ratio of 1:6:4. The samples were reacted at 800 °C for 6 days with prior heating at 300 °C for 1 day, and then allowed to cool slowly to room temperature. Prism-shaped single crystals of $K_3Mg_{18}Tt_{11}$ (Tt=Sn, Pb) were obtained from the reaction products. Both compounds are air and moisture-sensitive. Microprobe elemental analyses on clean surfaces of several single crystals of $K_3Mg_{18}Sn_{11}$ and $K_3Mg_{18}Pb_{11}$ gave K/Mg/Tt molar ratios of 3.0(8):18.5(7):11.4(6) and 3.0(7):18.4(6):11.3(6), respectively, which were in agreement with those determined by single-crystal X-ray diffraction studies. After the single-crystal X-ray diffraction analyses, single phases of $K_3Mg_{18}Tt_{11}$ (Tt=Sn, Pb) were prepared by reacting the stoichiometric mixture of the corresponding elements at 800 °C for 3 days, and then annealed at 520 °C for 6 days. The purities of the samples were confirmed by the X-ray diffraction powder studies (see Appendix A).

2.4. Crystal structure determination

Single crystals of $K_2Mg_{5-x}Sn_3$ ($x=0.28$), $K_3Mg_{18}Sn_{11}$ and $K_3Mg_{18}Pb_{11}$ were selected from the reaction products and sealed into thin-walled glass capillaries within the glove-box. Data collections for three compounds were performed on Rigaku Mercury CCD (Mo $K\alpha$ radiation, graphite monochromator) at 293(2) K. All three data sets were corrected for Lorentz factor, polarization, air absorption and absorption due to the variations in the path length through the detector faceplate. Absorption corrections based on multi-scan method were also applied [52].

All three structures were solved by using direct methods (SHELXTL) and refined by least-squares methods with atomic coordinates and anisotropic parameters [53]. $K_2Mg_{5-x}Sn_3$ ($x=0.28$) crystallized in the tetragonal space group $I4/mmm$ (No. 139) based on systematic absences, E-value statistics and satisfactory refinements. Site occupancy refinements indicated that all sites were fully occupied except Mg2 site with occupancy factor of 0.72(0). For $K_3Mg_{18}Tt_{11}$ (Tt=Sn, Pb), among the possible space groups, $P6_3/m$ (No. 176) was chosen for structural refinements. After all the sites were anisotropically refined, the final refinements converged at reliable $R1$ and $wR2$ ($I>2\sigma(I)$) factors of 0.0435, 0.0906 for $K_3Mg_{18}Sn_{11}$, and 0.0352, 0.0818 for $K_3Mg_{18}Pb_{11}$, respectively. However, we found that the anisotropic displacement parameters of the $Tt1$ site (4e) along the 6_3 axis were exceptionally larger than those of other directions. On the other hand, two slightly high residual peaks remaining in the subsequent difference-Fourier maps were found abnormally close to this position along the 6_3 axis. Considering the coordination environment of the 4e site, this site and two neighboring residual peaks were defined as Tt atom with free occupation factors, the condition that must be satisfied is $k_{Tt1a}+k_{Tt1b}+k_{Tt1c}=1$, where k is the occupancy. The results showed that the displacement parameter of these $Tt1$ sites greatly decrease to reasonable values and the anisotropic displacement parameters were also similar along different directions. Moreover with this model, the final $R1$ factors and difference-Fourier residues also evidently decrease. The refined occupancies of $Sn1a$, $Sn1b$, $Sn1c$ and $Pb1a$, $Pb1b$, $Pb1c$ positions converged to 0.739(3), 0.181(9), 0.080(8), and 0.689(4), 0.217(11), 0.095(10), respectively. Hence, we will use $Tt1a$ atom for discussion in detail as a representative in the paper. We also tried other methods, such as replacing 4e site with other atoms or mixing different atoms at this position, but the results indicated these strategies did not make any sense. Furthermore, some of the lower symmetry space group ($P6_3$, P-6, or $P6/m$) were also considered, but these did not support ordered models and satisfactory results. Such disorder maybe because the $Tt1$ atom is located in the 1D tunnel and has lower coordination numbers along the 6_3 axis comparing with other directions. This phenomena has also been observed in $Ba_2Mg_{12}Ge_{7.33}$ and many other phases with $P6_3/m$ space group containing 1D hexagonal channels [45,54–57].

Data collection and refined parameters for the three compounds are summarized in Table 1. Atomic coordinates and important bond lengths are listed in Tables 2 and 3, respectively. More details about crystallographic studies and anisotropic displacement parameters are given in Appendix A. Further data in the form of a crystallographic information file (CIF) can be obtained from the Fachinformationszentrum Karlsruhe, 76344 Eggenstein-Leopoldshafen, Germany (fax: +49 7247 808 666; e-mail: crysdata@fiz-karlsruhe.DE) on quoting the depository numbers: CSD-421342 ($K_2Mg_{5-x}Sn_3$ ($x=0.28$)), CSD-421343 ($K_3Mg_{18}Pb_{11}$) and CSD-421344 ($K_3Mg_{18}Sn_{11}$).

2.5. Computational details

To better understand the chemical bonding of the three compounds, electronic structure calculations were performed by both tight-binding linear muffin-tin orbital (TB-LMTO) method and extended Hückel tight-binging (EHTB) method.

The Stuttgart LMTO program: this program follows the TB-LMTO method in the local density and atomic sphere (ASA) approximations [58–61]. Interstitial spheres were introduced in the past to achieve space filling. ASA radii as well as positions and

Table 1
Crystal data and structure refinements for $K_2Mg_{5-x}Sn_3$ ($x=0.28$) and $K_3Mg_{18}Tt_{11}$ (Tt=Sn, Pb).

Chemical formula	$K_2Mg_{5-x}Sn_3$	$K_3Mg_{18}Sn_{11}$	$K_3Mg_{18}Pb_{11}$
fw	549.01	1860.47	2833.97
Space group	*I*4/*mmm* (No. 139)	$P6_3/m$ (No. 176)	$P6_3/m$ (No. 176)
a (Å)	4.9461(4)	11.8429(6)	11.9615(6)
c (Å)	23.403(3)	13.813(1)	13.909(1)
V (Å^3)	572.52(1)	1677.8(2)	1723.4(2)
Z	2	2	2
Crystal size (mm)	$0.40\times0.40\times0.10$	$0.40\times0.20\times0.20$	$0.16\times0.05\times0.05$
D_{calcd} (g cm^{-3})	3.185	3.683	5.461
Temperature (K)	293(2)	293(2)	293(2)
h k l ranges	(−5, 6), ±6, (−30, 26)	(−13,15), (−15,14), ±17	±15, (−14, 15), ±18
μ (mm^{-1})	7.409	8.741	54.196
Reflections collected	2067	11,198	13,209
Unique reflections	240	1340	1373
Reflections ($I>2\sigma(I)$)	236	1267	1077
GOF on F^2	1.107	1.125	1.177
*R*1, *wR*2 ($I>2\sigma(I)$)[a]	0.0241/0.0617	0.0412/0.0765	0.0342/0.0803
*R*1, *wR*2 (all data)	0.0245/0.0620	0.0445/0.0782	0.0474/0.0868
$\Delta\rho_{max}$ (e/Å^3)	0.93	2.98	3.58
$\Delta\rho_{min}$ (e/Å^3)	−1.12	−1.53	−2.65

[a] $R1=\sum\|F_o|-|F_c\|/\sum|F_o|$, $wR2=\{\sum w[(F_o)^2-(F_c)^2]^2/\sum w[(F_o)^2]^2\}^{1/2}$.

Table 2
Atomic coordinates and equivalent isotropic displacement parameters (Å$^2\times10^3$) for $K_2Mg_{5-x}Sn_3$ ($x=0.28$) and $K_3Mg_{18}Tt_{11}$ (Tt=Sn, Pb).

Atom	*Wyck*off	Occupancy	*x*	*y*	*z*	*U*(eq)[a]
$K_2Mg_{5-x}Sn_3$						
K1	4*e*	1	0	0	0.1993(1)	27(1)
Mg1	8*g*	1	1/2	0	0.0787(1)	24(1)
Mg2	2*b*	0.72(0)	1/2	1/2	0	27(1)
Sn1	2*a*	1	0	0	0	16(1)
Sn2	4*e*	1	1/2	1/2	0.1409(1)	22(1)
$K_3Mg_{18}Sn_{11}$						
K1	4*f*	1	1/3	2/3	0.5827(2)	19(1)
K2	2*c*	1	2/3	1/3	3/4	20(1)
Mg1	6*h*	1	0.2575(3)	0.1461(3)	3/4	18(1)
Mg2	12*i*	1	0.1230(2)	0.2702(2)	0.5833(2)	12(1)
Mg3	6*h*	1	0.0579(3)	0.4323(3)	3/4	15(1)
Mg4	12*i*	1	0.4337(2)	0.3773(2)	0.5837(2)	14(1)
Sn1a	4*e*	0.739(3)	0	0	0.6355(5)	16(1)
Sn1b	4*e*	0.181(9)	0	0	0.668(1)	16(1)
Sn1c	4*e*	0.080(8)	0	0	0.598(2)	16(1)
Sn2	12*i*	1	0.4083(1)	0.1134(1)	0.5839(1)	11(1)
Sn3	6*h*	1	0.2995(1)	0.4135(1)	3/4	11(1)
$K_3Mg_{18}Pb_{11}$						
K1	4*f*	1	1/3	2/3	0.5825(3)	9(1)
K2	2*c*	1	2/3	1/3	3/4	11(1)
Mg1	6*h*	1	0.2509(5)	0.1437(4)	3/4	9(1)
Mg2	12*i*	1	0.1212(3)	0.2710(3)	0.5826(2)	9(1)
Mg3	6*h*	1	0.0562(5)	0.4315(4)	3/4	6(1)
Mg4	12*i*	1	0.4325(3)	0.3780(3)	0.5842(2)	6(1)
Pb1a	4*e*	0.689(4)	0	0	0.6330(6)	7(1)
Pb1b	4*e*	0.217(11)	0	0	0.8949(8)	7(1)
Pb1c	4*e*	0.095(10)	0	0	0.667(2)	7(1)
Pb2	12*i*	1	0.4111(1)	0.1160(1)	0.5846(1)	3(1)
Pb3	6*h*	1	0.2991(1)	0.4159(1)	3/4	3(1)

[a] *U*(eq) is defined as one-third of the trace of the orthogonalized U_{ij} tensor.

Table 3
Selected bond lengths (Å) for $K_2Mg_{5-x}Sn_3$ ($x=0.28$) and $K_3Mg_{18}Tt_{11}$ (Tt=Sn, Pb).

$K_2Mg_{5-x}Sn_3$			
K1–Sn2	3.739(3)	Mg2–Mg1	3.085(2) × 8
K1–Mg1	3.751(2) × 4	Mg2–Sn2	3.2975(8) × 2
K1–Sn2	3.7552(8) × 4	Mg2–Sn1	3.4974(3) × 4
Mg1–Sn1	3.085(2) × 2	Mg1–Sn2	2.869(1) × 2
$K_3Mg_{18}Sn_{11}$			
K1–Sn3	3.645(2) × 3	Mg2–Sn1a	2.867(3)
K1–Sn2	3.670(2) × 3	Mg2–Sn1b	3.014(6)
K1–Mg4	3.822(3) × 3	Mg2–Sn1c	2.782(3)
K1–Mg3	3.825(3) × 3	Mg2–Sn2	2.956(2)
K2–Sn2	3.6670(5) × 6	Mg2–Sn2	2.969(2)
K2–Mg4	3.821(2) × 6	Mg2–Sn3	3.001(2)
Mg1–Sn1a	3.085(5) × 2	Mg3–Sn3	2.902(3)
Mg1–Sn1b	2.879(6) × 2	Mg3–Sn2	2.954(2) × 2
Mg1–Sn1c	3.383(2) × 2	Mg3–Sn3	2.978(3)
Mg1–Sn2	3.050(2) × 2	Mg4–Sn2	2.935(2)
Mg1–Sn3	2.949(3)	Mg4–Sn3	2.944(2)
Sn1a–Sn1a	3.163(1)	Mg4–Sn2	2.965(2)
		Mg4–Sn2	2.987(2)
$K_3Mg_{18}Pb_{11}$			
K1–Pb3	3.656(2) × 3	Mg2–Pb1a	2.898(4)
K1–Pb2	3.682(2) × 3	Mg2–Pb1b	2.830(4)
K1–Mg4	3.873(4) × 3	Mg2–Pb1c	3.047(1)
K1–Mg3	3.874(4) × 3	Mg2–Pb2	2.992(3)
K2–Pb2	3.6674(4) × 6	Mg2–Pb2	3.010(3)
K2–Mg4	3.866(3) × 6	Mg2–Pb3	3.043(3)
Mg1–Pb1a	3.075(6) × 2	Mg3–Pb3	2.929(4)
Mg1–Pb1b	3.297(8) × 2	Mg3–Pb2	2.973(3) × 2
Mg1–Pb1c	2.853(1) × 2	Mg3–Pb3	3.002(5)
Mg1–Pb2	3.116(3) × 2	Mg4–Pb2	2.959(3)
Mg1–Pb3	3.010(5)	Mg4–Pb3	2.967(3)
Pb1a–Pb1a	3.255(2)	Mg4–Pb2	3.004(3)
		Mg4–Pb2	3.014(3)

radii of additional empty spheres were calculated automatically. The basic set included the 4*s*, 4*p*, 3*d* orbitals for K; 3*s*, 3*p*, 3*d* orbitals for Mg; 5*s*, 5*p*, 4*d* and 4*f* orbitals for Sn; 6*s*, 6*p*, 5*d* and 5*f* orbitals for Pb atoms. The K 4*p*, 3*d*; Mg 3*p*, 3*d*; Sn 4*d*, 4*f*; and Pb 5*d*, 5*f* orbitals were treated with the down-folding technique [62]. In all cases, the *k*-space integrations were performed by the tetrahedron method [63]. The Fermi level was selected as the energy reference (E_F=0 eV).

EHTB calculations: semiempirical EHTB band calculations for the three compounds allowed Mulliken atom population analyses, which provided some guidance as to charge segregation within the framework [64]. The electronic calculations were carried out without K on the network of $[Mg_5Sn_3]^{2-}$ and $[Mg_{18}Tt_{11}]^{3-}$ for "$K_2Mg_5Sn_3$" model and $K_3Mg_{18}Tt_{11}$ (Tt=Sn, Pb), respectively. The following orbital energies and exponents were employed in the calculations (H_{ij}=orbital energy (eV), ξ=Slater exponent): Mg 3*s*, $H_{ij}=-9.00$,

ξ=1.10; 3*p*, H_{ij}= −4.50, ξ=1.10; Sn, 5*s*, H_{ij}= −16.20, ξ=2.12; 5*p*, H_{ij}= −8.32, ξ=1.82; Pb, 6*s*, H_{ij}= −15.70, ξ=2.35; 6*p*, H_{ij}= −8.00, ξ=2.06.

3. Results and discussion

3.1. Structural descriptions

Exploratory studies in the ternary K–Mg–*Tt* system lead to the discovery of three new polar intermetallic phases, namely, $K_2Mg_{5-x}Sn_3$ (x=0.28) and $K_3Mg_{18}Tt_{11}$ (*Tt*=Sn, Pb). Their structures feature 2D layer and 3D network, respectively, based on dominant Mg–*Tt* or/and *Tt*–*Tt* bonding interaction/s with K atoms as spacers.

$K_2Mg_{5-x}Sn_3$ (x=0.28) is isostructural with $Ni_{7-x}SbQ_2$ ($x\approx1.3$, *Q*=Se, Te) series with *Q* site (4*e*) replaced by Sn2, Sb site (2*b*) substituted by Sn1, the Ni site (8*g*) replaced by Mg1, the Ni site (2*a*) replaced by Mg2 and the remaining Ni site replaced by K atoms (Fig. 1) [65]. Such structure type has also been reported in several other phases, such as $Ni_{7-x}TtQ_2$ (*Tt*=Si, Ge, Sn, *Q*=Se, Te) and $Pd_{7-x}SnTe_2$ [66–68].

The structure of $K_2Mg_{5-x}Sn_3$ features 2D corrugated [Mg_5Sn_3] layers, which are separated by K^+ cations (Fig. 1). There are one K, two Mg and two Sn atoms in the asymmetric unit of $K_2Mg_{5-x}Sn_3$. As shown in Fig. 1, Mg1 atom is surrounded by two Sn1 and two Sn2 atoms with a slightly distorted tetrahedral geometry; and these [$MgSn_4$] tetrahedra are fused via edge-sharing into a 2D corrugated [Mg_2Sn_2] layer. Similar corrugated layer has also been reported in $ThCr_2Si_2$-type phases, such as $CaTM_2Ge_2$ (*TM*=Mn, Co–Zn), $SmPd_2Ge_2$, $BaZn_2Ge_2$, etc. [69–71]. Two adjacent [Mg_2Sn_2] layers are further condensed along the *c*-axis into a [Mg_4Sn_3] double layer via sharing Sn1 atoms, and form 1D narrow tunnels along the *b*-axis. The Mg2 atoms are located inside these tunnels, where weak Mg–Sn and Mg–Mg bonds also occur, leading to a [Mg_5Sn_3] layer. The Sn1 atom is surrounded by eight Mg1 atoms, whereas the Sn2 atom is coordinated with four Mg1 atoms.

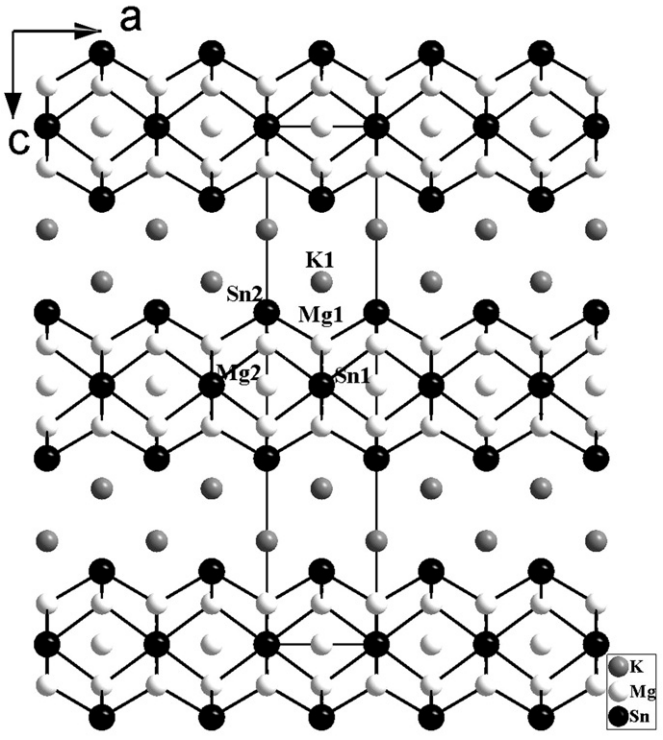

Fig. 1. View of the structure of $K_2Mg_{5-x}Sn_3$ along the *b*-axis. The K, Mg and Sn atoms are drawn as gray, white and blacks spheres, respectively.

The Mg1–Sn distances are in the range 2.869(1)–3.085(2) Å, which are slightly longer than the sum of the covalent radii of 2.799 Å, indicating evident Mg–Sn interactions [72]. These values compare well with those reported in related phases, such as CaMgSn (2.864–3.023 Å) [34], $Ca_{6.2}Mg_{3.8}Sn_7$ [44] and YbMgSn (2.916–3.022 Å) [73]. Mg2–Sn distances are in the range 3.2975(8)–3.4974(3) Å, which are significantly longer than the Mg1–Sn bonds. The K atoms are located at the interlayer space. Each potassium atom is coordinated by four Mg1 and five Sn2 atoms (Fig. S1, Appendix A). The K–Mg1 distance is 3.751(2) Å, and K–Sn bond lengths are in the range 3.739(3)–3.7552(8) Å, which are comparable with those reported in binary potassium stannides, such as K_8Sn_{25} [20].

The structure of $K_2Mg_{5-x}Sn_3$ is closely related to that of $BaMg_2Sn_2$ (*P*4/*nmm*, No. 129) and $BaMg_4Tt_3$ (*P*4/*mmm*, No. 123, *Tt*=Si, Ge) [34–35]. All these structures feature Mg–*Tt* network based on corrugated [Mg_2Tt_2] layers (Fig. 2). In $BaMg_2Sn_2$, adjacent [Mg_2Sn_2] layers are directly interconnected via Mg–Sn and Sn–Sn bonds into a 3D framework with 1D hexagonal tunnels, which are occupied by Ba^{2+} cations. In the structures of $BaMg_4Tt_3$ and $K_2Mg_{5-x}Sn_3$, two adjacent [Mg_2Tt_2] layers are fused into a [Mg_4Tt_3] double layer along the *c*-axis via sharing neighboring *Tt* atoms. In $BaMg_4Tt_3$, the [Mg_4Tt_3] double layers are directly interconnected via *Tt*–*Tt* bonds into the 3D framework with 1D hexagonal tunnels, which are occupied by Ba^{2+} cations. In $K_2Mg_{5-x}Sn_3$, the [Mg_4Sn_3] double layers are well separated by K^+ cations. In addition, the [Mg_4Sn_3] double layers in $K_2Mg_{5-x}Sn_3$ contain [Mg_2Sn_2] four member rings forming 1D tunnels larger than those in $BaMg_4Tt_3$. The former ones encapsulate additional Mg atoms, whereas the latter ones remain empty (Fig. 2).

The structure of $K_3Mg_{18}Tt_{11}$ (*Tt*=Sn, Pb) is closely related to the $Ho_2Rh_{12}As_7$ structural type [74], which is also known for other relevant germanide, such as $Ba_2Mg_{12}Ge_{7.33}$ [45]. Its structure features 3D [$Mg_{18}Tt_{11}$] framework composed of 1D hexagonal [$Mg_{18}Tt_{11}$] columns that are interconnected via exo Mg–*Tt* bonds, forming 1D hexagonal tunnel along the *c*-axis, which are occupied by K atoms (Fig. 3). Since the two compounds are isostructural, the structure of $K_3Mg_{18}Sn_{11}$ will be discussed in detail as a representative.

There are two K, four Mg and three Sn sites in the asymmetric unit of $K_3Mg_{18}Sn_{11}$. As shown in Fig. 4, all the Mg atoms and Sn2, Sn3 atoms are interconnected via Mg–Sn bonds to form 1D [MgSn] ladders, which are appreciably similar to those reported in CaMgSn [34] and $Ba_2Mg_{12}Ge_{7.33}$ [45]. Six adjacent [MgSn] ladders are fused via sharing Sn atoms into a [$Mg_{18}Sn_9$] column, along the *c*-axis, with 1D large tunnels based on [Mg_6Sn_6] rings. The Sn1 atoms form [Sn_2] dimers, which are aligned along the *c*-axis with longer inter-dimer Sn1…Sn1 distances of 3.743 Å. The Sn1–Sn1 bond distance within the [Sn_2] dimer is 3.163(1) Å, which is comparable to those in $Ca_{36}Sn_{23}$ (3.070 and 3.173 Å) and $Yb_{36}Sn_{23}$ (3.098 and 3.156 Å) [25,26]. All the [Sn_2] dimers are located at the above 1D tunnels of the [$Mg_{18}Sn_9$] columns, where the Mg–Sn1 bonds also occur, leading to the [$Mg_{18}Sn_{11}$] columns along the *c*-axis. These [$Mg_{18}Sn_{11}$] columns are further interconnected via exo Mg–Sn bonds into the 3D [$Mg_{18}Sn_{11}$] framework, forming 1D hexagonal tunnel made by [Mg_3Sn_3] six-membered rings along the *c*-axis, which are filled by K atoms (Fig. 3). Both K1 and K2 atoms are surrounded by twelve Sn atoms with a hexagonal prismatic geometry (Fig. S2, Appendix A). The K–Mg and K–Sn distances are in the ranges 3.822(3)–3.825(3) Å and 3.645(2)–3.670(2) Å, respectively, which are comparable to those in $K_2Mg_{5-x}Sn_3$.

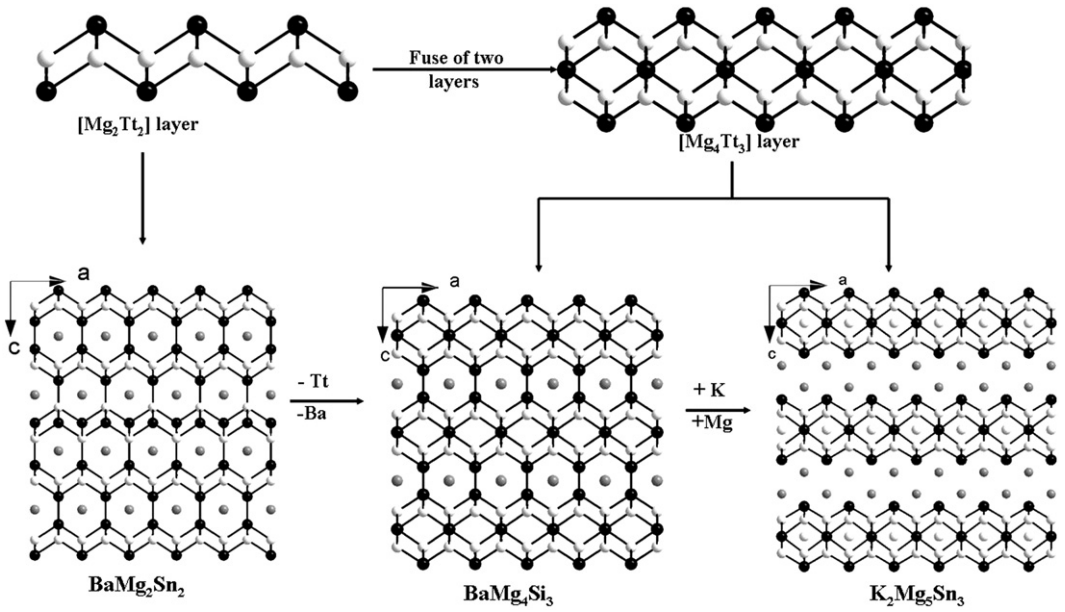

Fig. 2. Comparing of the structures of $BaMg_2Sn_2$, $BaMg_4Si_3$ and $K_2Mg_{5-x}Sn_3$ along the *b*-axis. The K (Ba), Mg and Sn (Si) atoms are drawn as gray, white and black spheres, respectively.

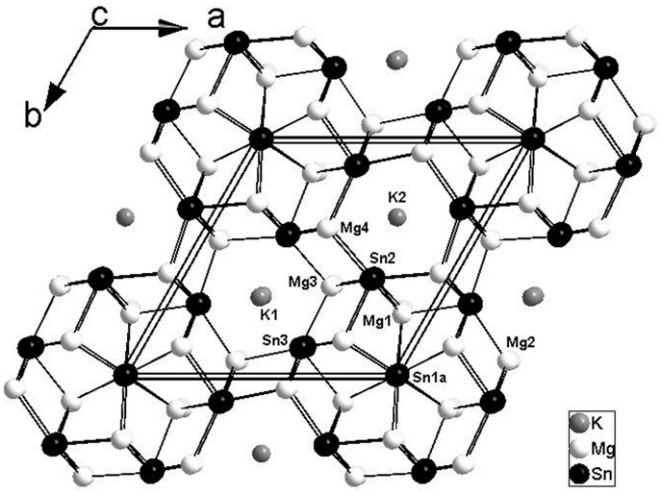

Fig. 3. View of the structure of $K_3Mg_{18}Sn_{11}$ along the *c*-axis. The K, Mg and Sn atoms are drawn as gray, white and blacks spheres, respectively.

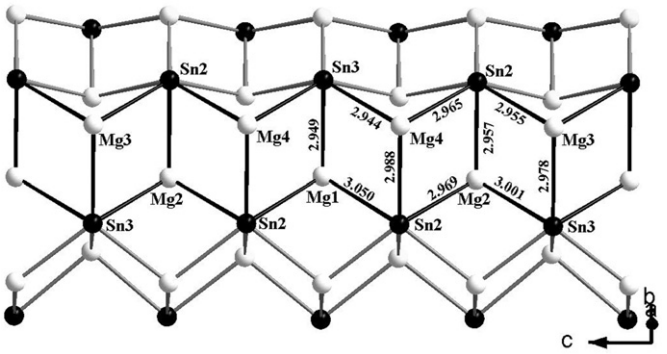

Fig. 4. View of the connecting manner of the [MgSn] ladders in $K_3Mg_{18}Sn_{11}$.

Mg1 atom is in a distorted [Sn_5] square pyramidal geometry. Mg2, Mg3 and Mg4 atoms are all surrounded by four Sn atoms with slightly distorted tetrahedral coordination geometries, which are similar to the Mg1 atom in $K_2Mg_{5-x}Sn_3$. The Mg–Sn bond distances are in the range 2.867(3)–3.085(5) Å, which are comparable to those of Mg1–Sn bonds in $K_2Mg_{5-x}Sn_3$. The Mg–Pb bond distances are in the range 2.898(4)–3.116(3) Å in $K_3Mg_{18}Pb_{11}$, which are comparable with those in $BaMg_2Pb_2$ [34].

3.2. Magnetic properties

Plots of the molar magnetic susceptibility χ_m of the three compounds as a function of temperature in the range 5–310 K are presented in Fig. S5 (see Appendix A). All three compounds exhibit essentially temperature-independent paramagnetic behavior over 10–300 K with susceptibilities of about 2.9×10^{-3}, 3.1×10^{-3} and 3.8×10^{-3} emu/mol for "$K_2Mg_5Sn_3$", $K_3Mg_{18}Sn_{11}$ and $K_3Mg_{18}Pb_{11}$, respectively. The slight increase of the molar susceptibility below 10 K probably arises from the presence of a small amount of paramagnetic impurities.

3.3. Electronic structures and chemical bonds

To understand the electronic structures and chemical bonding of the title compounds, the first-principle electronic calculations were carried out for all three compounds using the TB-LMTO-ASA method. The electronic structure calculations were carried out for idealized "$K_2Mg_5Sn_3$" model, where the Mg2 site was assumed to be fully occupied. The total density of states (TDOS) and partial density of states (PDOS) for "$K_2Mg_5Sn_3$" are shown in Fig. 5a. The Fermi level fall in a pronounced pseudo-gap, which indicates the compound shows the semimetallic behavior. This pseudo-gap separates bonding from antibonding states, which show "$K_2Mg_5Sn_3$" has an optimum electron count. The states below the Fermi level (0 to −9 eV) are mainly the contributions from Mg and Sn atoms, and the strong hybridization between Mg and Sn states indicates significant Mg–Sn bonding. Most of the densities of 4*s* states of the K atoms are located above the Fermi level, indicating that they are mainly electron donors.

For further analyses of bonding interactions between atom types, crystal orbital Hamilton population (–COHP) as well as integrated –COHP (–ICOHP) analyses are evaluated (Fig. 5b). The strongest

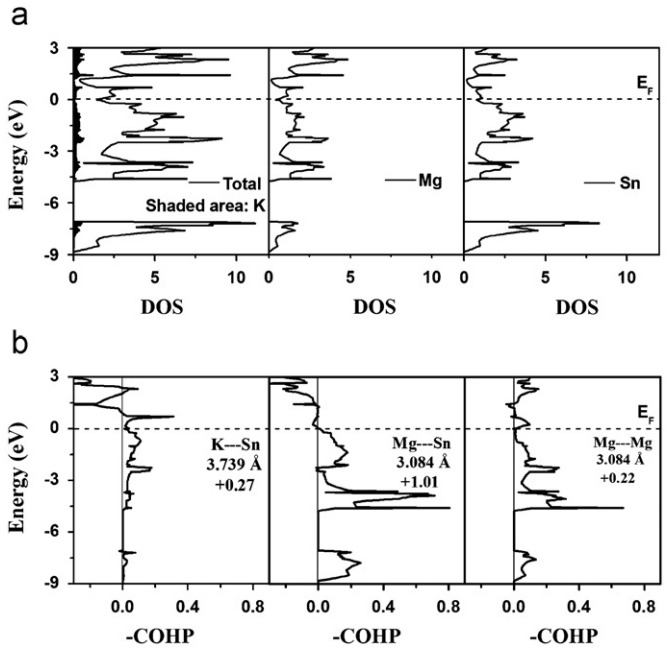

Fig. 5. TB-LMTO-ASA electronic structure calculation results for "$K_2Mg_5Sn_3$". (a) Total DOS (black) and partial DOS curve. (b) –COHP curves for three different interactions: K–Sn, Mg–Sn and Mg–Mg bonds. The integrated values for the overlap –ICOHP per bond up to the Fermi level (dashed line) and the corresponding distances are given. The dashed lines denote the Fermi level.

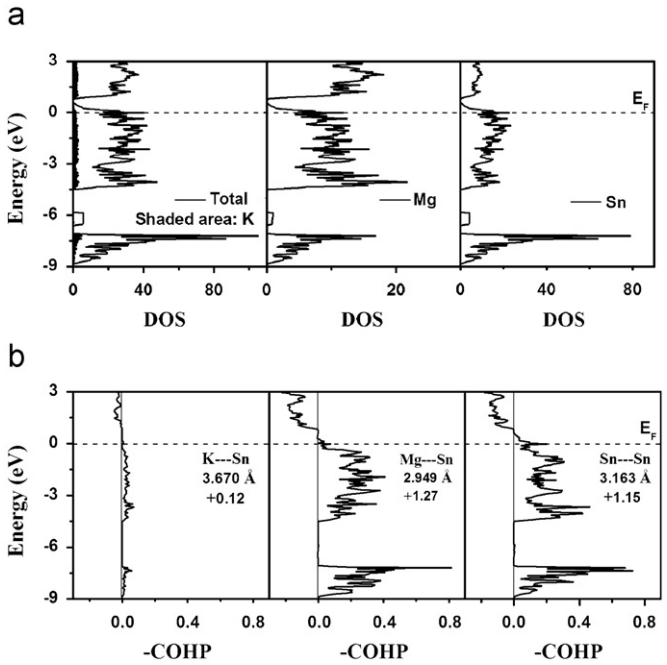

Fig. 6. TB-LMTO-ASA electronic structure calculation results for $K_3Mg_{18}Sn_{11}$. (a) Total DOS (black) and partial DOS curves. (b) –COHP curves for three different interactions: K–Sn, Mg–Sn and Sn–Sn bonds. The integrated values for the overlap –ICOHP per bond up to the Fermi level (dashed line) and the corresponding distances are given.

bonding interaction occurs for Mg1–Sn bonds (2.869(1) and 3.085(1) Å) with –ICOHP values of 1.71 and 1.01 eV/bond, respectively, which are much stronger than those of Mg2–Sn bonds (3.2975(8) and 3.4974(3) Å) with –ICOHP values of 0.31 and 0.21 eV/bond, respectively. Mulliken atom population analyses based on EHTB calculations are also performed, and such calculation strategy has been effectively used in many cases [75–77]. The calculated Mulliken charges for Mg1 and Mg2 atoms are approximately +0.52 and +1.11, respectively (Table S3, Appendix B). The former value is notably smaller than latter. Considering both the results of the LMTO and EHTB calculations as well as the coordination environments of Mg atoms, two independent Mg atoms show some different roles in the structure of "$K_2Mg_5Sn_3$". The Mg1 atom mainly show substantial participation in the overall "$[Mg_5Sn_3]$" layers along with Sn atoms, whereas the Mg2 atom acts more as a spacer and shows a greater electron donor character comparing with Mg1 atom. Similar calculation strategy has also been used in several phases, such as Mg_2Zn_{11} and $Mg_2Cu_6Ga_5$ [78,79].

LMTO calculation results for $K_3Mg_{18}Sn_{11}$ and $K_3Mg_{18}Pb_{11}$ are very similar, and principally only the former will be used to rationalize the chemical bonding. As shown in the TDOS and PDOS of $K_3Mg_{18}Sn_{11}$ in Fig. 6a, the Fermi level almost cuts through the top of the valence bands, separated from the upper conduction bands by 0.7 eV, indicating a metallic behavior of the compound. So the compound $K_3Mg_{18}Sn_{11}$ can be termed as hypoelectronic. Similar to the "$K_2Mg_5Sn_3$", the states below the Fermi level (0 to −9 eV) are mainly dominated by Mg and Sn atoms, and the contributions of K atoms are very small. There is also strong hybridization between Mg and Sn atoms in $K_3Mg_{18}Sn_{11}$, hence significant Mg–Sn bond interactions are expected. The crystal orbital Hamilton population (COHP) curves indicate that the Mg–Sn and Sn–Sn bonding interactions are not optimized at the Fermi level, which show that there are electron deficiencies locating at the Mg–Sn and Sn–Sn bonds (Fig. 6b). The Mg–Sn and Sn–Sn bonds have much larger –ICOHPs of 0.72–1.45 and 1.15 eV/bond, respectively, compared with those of the K–Sn bonds (0.12–0.14 eV/bond). The calculated Mulliken charges of Mg1, Mg2, Mg3 and Mg4 are +0.70, +0.58, +0.44 and +0.46 for $K_3Mg_{18}Sn_{11}$, and +0.64, +0.51, +0.36 and +0.39 for $K_3Mg_{18}Pb_{11}$, respectively. These values are similar to the Mg1 atom in "$K_2Mg_5Sn_3$". Both LMTO and EHTB calculations as well as the structural analyses indicate that Mg mainly shows substantial participation in the overall bonding of the structure and forms a 3D Mg–Sn framework, and K acts more as an electron donor. Such multifunctional roles of Mg atom have also been reported in many ternary systems involving Mg and p-elements, such as $K_3Mg_{20}In_{14}$ [80] and $AeMg_5In_3$ (Ae=Ba, Sr) [81].

4. Concluding remarks

In summary, we have successfully obtained three new ternary intermetallics, namely, $K_2Mg_{5-x}Sn_3$ (x=0.28) and $K_3Mg_{18}Tt_{11}$ (Tt=Sn, Pb). The structure of $K_2Mg_{5-x}Sn_3$ (x=0.28) features a 2D corrugated $[Mg_5Sn_3]$ layer with K^+ cations as spacers, whereas the structure of $K_3Mg_{18}Tt_{11}$ (Tt=Sn, Pb) features a 3D $[Mg_{18}Sn_{11}]$ network with 1D hexagonal tunnels occupied by the K^+ cations. In these structures, Mg atoms can function either as an electron donor or participator in the network along with Tt atoms, whereas all the K atoms are encapsulated in the Mg–Tt network and act more as electron donors. Results of our work demonstrate that mixing of alkali and alkaline earth metals is a very effective route to explore new phases due to the different sizes and valence electron count. It is expected that many other new intermetallic phases with novel structures can be found in other A–Mg–Tt systems.

Acknowledgment

We thank the financial supports from the Youth Science Foundation of Jining University (2009QNKJ07).

Appendix A. Supplementary materials

Supplementary materials associated with this article can be found in the online version at doi:10.1016/j.jssc.2011.02.003.

Tables of anisotropic displacement parameters, selected bond lengths and the corresponding –ICOHP values, and calculated Mulliken charges of atoms, figures showing the coordination geometries around K and Mg atoms, molar magnetic susceptibilities and simulated and experimental XRD patterns.

References

[1] G.J. Miller, in: S.M. Kauzlarich (Ed.), Chemistry, Structure and Bonding of Zintl Phases and Ions, VCH Publishers, New York, 1996, p. 1.
[2] B. Eisenmann, G. Cordier, in: S.M. Kauzlarich (Ed.), Chemistry, Structure and Bonding of Zintl Phases and Ions, VCH Publishers, New York, 1996, p. 61.
[3] J.D. Corbett, in: S.M. Kauzlarich (Ed.), Chemistry, Structure and Bonding of Zintl Phases and Ions, VCH Publishers, New York, 1996, p. 139.
[4] J.D. Corbett, Angew. Chem. Int. Ed. 39 (2000) 670.
[5] T.F. Fässler, S. Hoffmann, Z. kristallogr. 214 (1999) 722.
[6] T.F. Fässler, Chem. Soc. Rev. 32 (2003) 80.
[7] T.F. Fässler, Angew. Chem. Int. Ed. 40 (2001) 22.
[8] B. Böhme, A.M. Guloy, Z.-J. Tang, W. Schnelle, U. Burkhardt, M. Baitinger, Y. Grin, J. Am. Chem. Soc. 129 (2007) 5348.
[9] V. Quéneau, E. Todorov, S.C. Sevov, J. Am. Chem. Soc. 120 (1998) 3263.
[10] V. Queneau, S.C. Sevov, Angew. Chem. Int. Ed. 36 (1997) 1754.
[11] H.G. von Schnering, J.L Ianos, J. -H. Chang, K. Peters, E. -M. Peters, R. Nesper, Z. Kristallogr. NCS 220 (2005) 324.
[12] C. Lupu, J.-G. Mao, J.W. Rabalais, A.M. Guloy, Inorg. Chem. 42 (2003) 3765.
[13] R. Nesper, Prog. Solid State Chem. 20 (1990) 1.
[14] T.F. Fässler, Z. Anorg. Allg. Chem. 632 (2006) 1125.
[15] J.T. Vaughey, J.D. Corbett, Inorg. Chem. 36 (1997) 4316.
[16] T.F. Fässler, S. Hoffmann, Inorg. Chem. 42 (2003) 5474.
[17] F. Dubois, M. Schreyer, T.F. Fässler, Inorg. Chem. 44 (2005) 477.
[18] T.F. Fässler, C. Kronseder, Angew. Chem. Int. Ed. 37 (1998) 1571.
[19] F. Springelkamp, R.A. de Groot, W. Geertsma, W. van der Lugt, F.M. Mueller, Phys. Rev. B. 32 (1985) 2319.
[20] J.-T. Zhao, J.D. Corbett, Inorg. Chem. 33 (1994) 5721.
[21] F. Dubois, T.F. Fässler, J. Am. Chem. Soc. 127 (2005) 3264.
[22] A. Kaltzoglou, S.D. Hoffmann, T.F. Fässler, Eur. J. Inorg. Chem. (2007) 4162.
[23] E. Todorov, S.C. Sevov, Inorg. Chem. 37 (1998) 3889.
[24] V. Queneau, S.C. Sevov, Inorg. Chem. 37 (1998) 1358.
[25] A.K. Ganguli, A.M. Guloy, E.A. Leon-Escamilla, J.D. Corbett, Inorg. Chem. 32 (1993) 4349.
[26] E.A. Leon-Escamilla, J.D. Corbett, Inorg. Chem. 38 (1999) 738.
[27] S. Hoffmann, T.F. Fässler, Inorg. Chem. 42 (2003) 8748.
[28] M.T. Klem, J.T. Vaughey, J.G. Harp, J.D. Corbett, Inorg. Chem. 40 (2001) 7020.
[29] S. Bobev, S.C. Sevov, Angew. Chem. Int. Ed. 39 (2000) 4108.
[30] S. Bobev, S.C. Sevov, Angew. Chem. Int. Ed. 40 (2001) 1507.
[31] S. Bobev, S.C. Sevov, Inorg. Chem. 39 (2000) 5930.
[32] S. Bobev, S.C. Sevov, J. Am. Chem. Soc. 121 (1999) 3795.
[33] B. Eisenmann, H. Schäfer, A. Weiss, Z. Anorg. Allg. Chem. 391 (1972) 241.
[34] B. Eisenmann, H. Schäfer, Z. Anorg. Allg. Chem. 403 (1974) 163.
[35] F. Zürcher, S. Wengert, R. Nesper, Inorg. Chem. 38 (1999) 4567.
[36] R. Nesper, F. Zürcher, Z. Kristallogr. NCS 214 (1999) 20.
[37] R. Nesper, F. Zürcher, Z. Kristallogr. NCS 214 (1999) 22.
[38] R. Kraft, R. Pöttgen, Monatsh. Chem. 135 (2004) 1327.
[39] P.H. Tobash, S. Bobev, J. Am. Chem. Soc. 128 (2006) 3532.
[40] R. Nesper, S. Wengert, F. Zürcher, A. Currao, Chem. Eur. J. 5 (1999) 3382.
[41] A. Currao, R. Nesper, Angew. Chem. Int. Ed. 37 (1998) 841.
[42] S. Wengert, R. Nesper, Z. Anorg. Allg. Chem. 624 (1998) 1801.
[43] R. Nesper, A. Currao, S. Wengert, Chem. Eur. J. 4 (1998) 2251.
[44] A.K. Ganguli, J.D. Corbett, M. Köckerling, J. Am. Chem. Soc. 120 (1998) 1223.
[45] F. Zürcher, R. Nesper, Z. Anorg. Allg. Chem. 628 (2002) 1581.
[46] R. Kraft, R. Pöttgen, Monatsh. Chem. 136 (2005) 1707.
[47] R. Nesper, S. Wengert, Monatsh. Chem. 130 (1999) 197.
[48] S. Wengert, R. Nesper, Inorg. Chem. 39 (2000) 2861.
[49] H. Pauly, A. Weiss, H. Witte, Z. Metallkd 59 (1968) 414.
[50] V.V. Pavlyuk, O.I. Bodak, Izv. Akad. Nauk SSSR, Neorg. Mater. 28 (1992) 988.
[51] R. Nesper, J. Curda, H.G.Von Schnering, J. Solid State Chem. 62 (1986) 199.
[52] CrystalClear version. 1.3.5; Rigaku Corporation, Woodlands, TX, 1999.
[53] G.M. Sheldrick, SHELXTL, Crystallographic Software Package, version 5.1; Bruker-Axs, Madison, W1, 1998.
[54] Y.M. Prots, W. Jeitschko, Inorg. Chem. 37 (1998) 5431.
[55] E. Gaudin, B. Chevalier, J. Solid State Chem. 180 (2007) 1397.
[56] Y.M. Prots, W. Jeitschkor, J. Solid State Chem. 137 (1998) 302.
[57] A.I. Tursina, A.V. Gribanov, Y.D. Seropegin, O.I. Bodak, J. Alloys Compd. 367 (2004) 142.
[58] O.K. Andersen, O. Jepsen, Phys. Rev. Lett. 53 (1984) 2571.
[59] O.K. Andersen, O. Jepsen, D. Glötzel, in: F. Bassani F., M.P. Fumi (Eds.), Highlights of Condensed Matter Theory, Tosi, North Holland, New York, , 1985.
[60] O. Jepsen, O.K. Andersen, The Stuttgart TB-LMTO Program, Version 4.7.
[61] U. Von Barth, L. Hedin, J. Phys. C 5 (1972) 1629.
[62] O.K. Andersen, Phys. Rev. B 62 (2000) R16219.
[63] P.E. Blöchl, O. Jepsen, O.K. Andersen, Phys. Rev. B 49 (1994) 16223.
[64] J. Ren, W. Liang, M.-H. Whangbo, CAESAR for Windows; Prime-Corlor Software Inc., North Carolina State University, Raleigh, NC, 1998.
[65] T.K. Reynolds, J.G. Bales, F.J. DiSalvo, Chem. Mater. 14 (2002) 4746.
[66] A.I. Baranov, A.A. Isaeva, L. Kloo, B.A. Popovkin, Inorg. Chem. 42 (2003) 6667.
[67] A.I. Baranov, A.A. Isaeva, L. Kloo, V.A. Kulbachinskii, R.A. Lunin, V.N. Nikiforov, B.A. Popovkin, J. Solid State Chem. 177 (2004) 3616.
[68] S.V. Savilov, A.N. Kuznetsov, B.A. Popovkin, V.N. Khrustalev, P. Simon, J. Getzschmann, T. Doert, M. Ruck, Z. Anorg. Allg. Chem. 631 (2005) 293.
[69] C. Kranenberg, D. Johrendt, A. Mewis, R. Pöttgen, G. Kotzyba, H. Trill, B.D. Mosel, J. Solid State Chem. 167 (2002) 107.
[70] W.M. Williams, R.T. Macaluso, M. Moldovan, D.P. Young, J.Y. Chan, Inorg. Chem. 42 (2003) 7315.
[71] D.M. Proserpio, G. Artioli, S. Mulley, G. Chacon, C. Zheng, Chem. Mater. 9 (1997) 1463.
[72] L. Pauling, B. Kamb, In: Proc. Natl. Acad. Sci. (USA) (1986) 356983 (1986) 3569.
[73] F. Merlo, M. Pani, M.L. Fornasini, J. Alloys Compd. 196 (1993) 145.
[74] J.Y. Pivan, R. Guérin, M. Sergent, J. Less-Common Met. 107 (1985) 249.
[75] C.-S. Lee, G.J. Miller, J. Am. Chem. Soc. 122 (2000) 4937.
[76] B. Li, J.D. Corbett, Inorg. Chem. 46 (2007) 8812.
[77] Q.-S. Lin, L.D. Corbett, Inorg. Chem. 46 (2007) 8722.
[78] S. Samson, Acta Chem. Scand. 3 (1949) 835.
[79] Q.-S. Lin, L.D. Corbett, Inorg. Chem. 42 (2003) 8762.
[80] B. Li, J.D. Corbett, Inorg. Chem. 45 (2006) 3861.
[81] B. Li, J.D. Corbett, Inorg. Chem. 46 (2007) 2237.